Tryptophan Scanning Mutagenesis in the αM3 Transmembrane Domain of the Torpedo californica Acetylcholine Receptor: Functional and Structural Implications

6 AUTHORS, INCLUDING:

Ricardo Martí-Arbona

Los Alamos National Laboratory

19 PUBLICATIONS   **344** CITATIONS

SEE PROFILE

Legier V Rojas

Central University of the Caribbean

37 PUBLICATIONS   **508** CITATIONS

SEE PROFILE

Article

Tryptophan Scanning Mutagenesis in the M3 Transmembrane Domain of the *Torpedo californica* Acetylcholine Receptor: Functional and Structural Implications

Gisila R. Guzmn, John Santiago, Ariamsi Ricardo, Ricardo Mart-Arbona, Legier V. Rojas, and Jos A. Lasalde-Dominicci

More About This Article

Additional resources and features associated with this article are available within the HTML version:

- Supporting Information
- Links to the 2 articles that cite this article, as of the time of this article download
- Access to high resolution figures
- Links to articles and content related to this article
- Copyright permission to reproduce figures and/or text from this article

View the Full Text HTML

Tryptophan Scanning Mutagenesis in the αM3 Transmembrane Domain of the *Torpedo californica* Acetylcholine Receptor: Functional and Structural Implications[†]

Gisila R. Guzmán,[‡] John Santiago,[‡] Ariamsi Ricardo,[‡] Ricardo Martí-Arbona,[‡] Legier V. Rojas,[§] and José A. Lasalde-Dominicci*,[‡]

Department of Biology, University of Puerto Rico, P.O. Box 23360, San Juan, Puerto Rico 00931-3360, and Department of Physiology, School of Medicine, Universidad Central del Caribe, Bayamón, Puerto Rico 00960-6032

Received May 9, 2003; Revised Manuscript Received August 14, 2003

ABSTRACT: The functional role of the αM3 transmembrane domain of the *Torpedo* nicotinic acetylcholine receptor (AChR) was characterized by performing tryptophan-scanning mutagenesis at 13 positions within αM3, from residue M278 through I290. The expression of the mutants in *Xenopus* oocytes was measured by [^{125}I]-α-bungarotoxin binding, and ACh receptor function was evaluated by using a two-electrode voltage clamp. Six mutants (L279W, F280W, I283W, V285W, S288W, and I289W) were expressed at lower levels than the wild type. Most of these residues have been proposed to face the interior of the protein. The I286W mutant was expressed at 2.4-fold higher levels than the wild type, and the two lipid-exposed mutations, F284W and S287W, were expressed at similar levels as wild type. Binding assays indicated that the αM3 domain can accommodate bulky groups in almost all positions. Three mutations, M282W, V285W, and I289W, caused a loss of receptor function, suggesting that the tryptophan side chains alter the conformational changes required for channel assembly or ion channel function. This loss of function suggests that these positions may be involved in helix−helix contacts that are critical for channel gating. The lipid-exposed mutation F284W enhances the receptor macroscopic response at low ACh concentrations and decreases the EC$_{50}$. Taken together, our results suggest that αM3 contributes to the gating machinery of the nicotinic ACh receptor and that αM3 is comprised of a mixture of two types of helical structures.

The nicotinic acetylcholine receptor (AChR) is a member of a family of ligand-gated ion channels present in excitable tissues. The AChR from *Torpedo californica* is an allosteric and integral membrane protein comprised of five subunits arranged pseudo-symmetrically in a stoichiometry of α₂βγδ (*1−3*). The amino acid sequences of the four subunits are all similar, suggesting that they have similar structures and have descended from a common genetic ancestor (*4*). Each subunit contains a large hydrophilic N-terminus, four transmembrane domains of 20−30 amino acids (M1−M4), a variable intracellular loop between M3 and M4, and a short extracellular C-terminus (*5*). The M2 segment contributes to the ion channel pore in the closed conformation, whereas both M1 and M2 contribute to the ion channel pore in its open conformation (*6*). The M3 and M4 segments are lipid-exposed domains, and the lipid-exposed residues of all the subunits have been mapped using photolabeling techniques (*7, 8*).

Site-directed mutagenesis of the αM4 transmembrane domain of the AChR has provided valuable information regarding AChR structure and function, particularly at the lipid-exposed positions (*9−16*). Mutation of the lipid-exposed residues αC418 and βC447 suggested that the hydrophobicity of these side chains is essential for stabilizing the open-channel conformation (*10*). Replacement of αC418 and αT422 with alanine in the muscle-type AChR increased the channel-closing rate (*14*), whereas mutations at T422 of the α and the ε subunits showed that this residue contributes to channel gating through hydrogen bonds (*15, 16*). In a previous study, tryptophan-scanning mutagenesis of the αM4 domain showed periodicity of functional changes at positions αC412 through αV425, suggesting that this region has an α helical structure (*13*).

Several residues of the *Torpedo* M3 transmembrane domains are in contact with the lipid interface (*8*), and these contacts are proposed to be distant from the pore (*17*). Photolabeling of the αM3 transmembrane domain of *Torpedo* using 3-trifluoromethyl-3-m-[^{125}I]-iodophenyldiazirine ([^{125}I]-TID) showed that the F284 and S287 residues are in contact with the lipid interface; the periodicity of these labeled residues suggested an α helical structure (*8*). Recent studies showed that the M3 transmembrane domain of the neuronal AChR is involved in ion-channel gating (*18*). Three-dimensional ¹H NMR studies of a synthetic peptide corre-

* Corresponding author. Tel.: (787) 764-0000 ext. 2765. Fax: (787) 753-3852. E-mail: joseal@coqui.net.
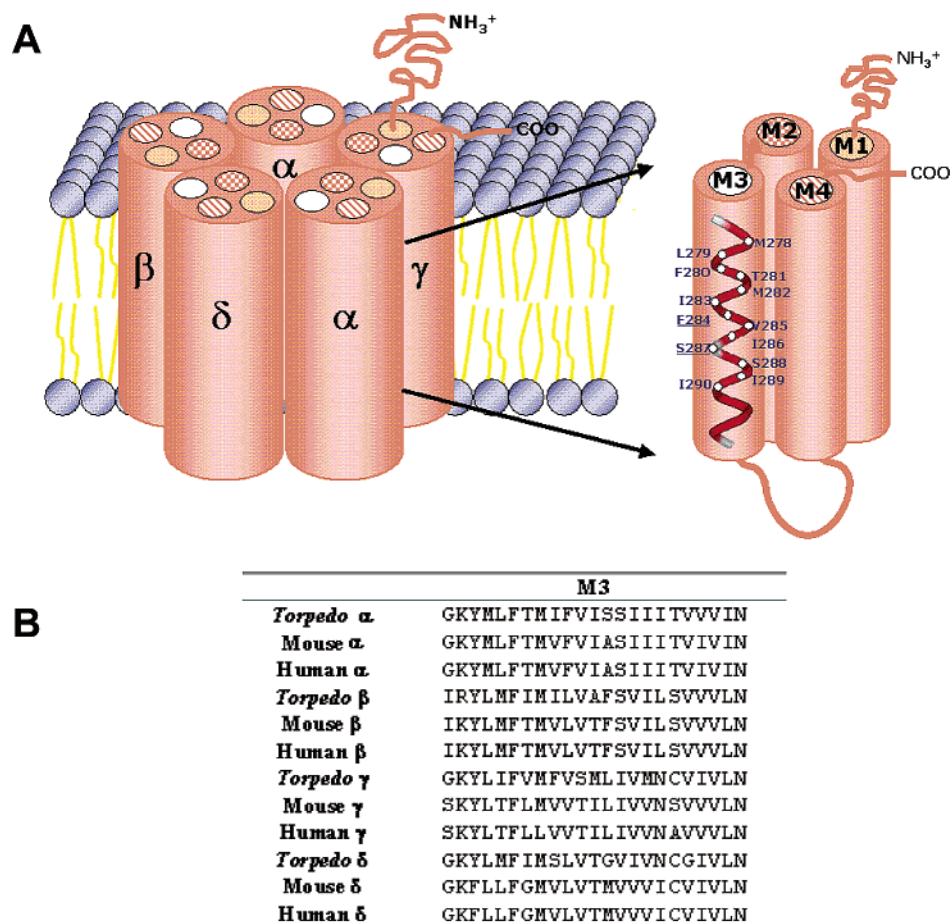‡ University of Puerto Rico.
§ Universidad Central del Caribe.

FIGURE 1: Topological representation of the αM3 domain of the AChR. (A) Tryptophan-scanning mutagenesis was performed starting from M278W and extending to I290W. Two lipid-exposed positions, F284 and S287 (underlined), were included in the analysis. (B) Alignment of M3 sequences for the five AChR subunits.

sponding to the αM3 transmembrane domain of *Torpedo* suggested that this region forms a right-handed helix (*19*). A kinetic analysis of a series of side-chain mutations on αV285 (a naturally occurring mutation in congenital myasthenic syndrome) showed that the M3 transmembrane domain is essential to the gating properties of muscle-type AChR (*20*). Mutational analysis of the AChR has been extended to the M3 transmembrane domain (*21−23*). Tryptophan substitutions in the lipid-exposed residues γF292 and γL296 increased the normalized macroscopic response of *Torpedo* AChR (*21*). More recently, de Rosa and colleagues demonstrated that the 8′ position of the M3 domain within each of the AChR subunits contributes to the mechanism of channel gating (*22*). Although these studies have provided extensive information about the M3 transmembrane domain, its secondary structure and its specific role in channel gating remain to be defined.

The aim of the present study is to examine the role of the αM3 transmembrane domain on channel function and to further characterize its secondary structure patterns. We performed tryptophan-scanning mutagenesis at 13 positions in the M3 domain of the *Torpedo* AChR α subunit (from residues M278 to I290, as shown in Figure 1). The expression levels of all the mutants were measured by iodinated α-bungarotoxin ([^{125}I]-α-BTX) binding, and the functional expression was assessed by two-electrode voltage clamp analysis. The findings show that the αM3 transmembrane domain plays a role in allosteric transitions of the AChR.

The periodicity of the functional response, as well as the normalized expression per volume change in each of these mutations, suggests that the αM3 transmembrane segment is comprised of a mixture of two types of helical structures.

METHODS

Mutations in the α Subunit. The αM3 mutants were prepared using the overlap extension method for sit-directed mutagenesis (*23*) and the Quick Change Site Directed Mutagenesis kit (Stratagene, La Jolla, CA). Mutagenic primers containing the desired codon replacement [TGG (Trp)] and extending 11−13 bases on each side of the mismatched region were synthesized by Life Technologies-Gibco BRL (Gaithersburg, MD). The PCR cycling protocol included denaturation of the plasmid for 30 s at 95 °C, primer annealing for 1 min at 55 °C, and extension for 12 min at 68 °C. After DNA amplification, the samples were digested with 10 units of *Dpn*I endonuclease at 37 °C for 1 h. The samples were then transformed into *Epicurian coli* XL1 supercompetent cells. The DNA was purified using the QIAprep Spin Miniprep kit (Qiagen, Germantown, MD) and subjected to sequence analysis.

In Vitro RNA Transcript Synthesis and Expression in Xenopus Oocytes. cDNA templates corresponding to the α, β, γ, and δ subunits of *Torpedo* AChR were linearized and subjected to in vitro transcription with the SP6 mMESSAGE mMACHINE kit (Ambion, Austin, TX). Briefly, RNA transcripts corresponding to the α, β, γ, and δ subunits in a

2:1:1:1 ratio were injected in *Xenopus* oocytes (10 ng/oocyte at a concentration of 0.2 μg/μL). The injected oocytes were incubated at 19 °C for 3 days in 0.5X Leibovitz's L-15 medium (Gibco BRL) supplemented with 400 μg/mL bovine serum albumin, 119 mg/mL penicillin, 200 mg/mL strepto-mycin, and 110 mg/mL pyruvic acid. The medium was replaced daily.

Voltage Clamp on Xenopus Oocytes. Oocytes were trans-ferred to a recording chamber and continuously perfused with MOR2 buffer (115 mM NaCl, 2.5 mM KCl, 1 mM Na$_2$-HPO$_4$, 5 mM MgCl$_2$, 0.2 mM CaCl$_2$, 0.5 mM EGTA, and 5 mM HEPES, pH = 7.4) at a rate of 15 mL/min. All reagents were from Sigma-Aldrich (St. Louis, MO). Currents were recorded from 3 to 4 days after mRNA injection at 20 °C using a voltage clamp with two microelectrodes and a GeneClamp 500B amplifier (Axon Instruments, Union City, CA). Membrane currents were digitized using the DigiData 1200 interface (Axon Instruments) and filtered at 2 kHz during recording. The Whole Cell Program 2.3 (provided by Dr. J. Dempster, University of Strathclyde, UK), running on a Pentium III-based computer, was used for data acquisi-tion. The data were analyzed with Prism 3.0 (GraphPad Software, San Diego, CA). Data points for dose−response curves were taken from peak current at six ACh concentra-tions (1, 3, 10, 30, 100, and 300 μM) from an average of 8−15 oocytes. Dose−response data were fitted using a curve of the form $Y = 100/(1 + (K_d/A)^n)$ and nonlinear regression curves. The EC$_{50}$ and Hill coefficient values for individual oocytes were averaged to generate final estimates. Statistical analysis was performed using Student's *t*-test in GraphPad Prism 3.0.

[^{125}I]-α-Bungarotoxin Binding Assay. The expression of AChR in oocyte membranes was assayed by measuring the binding of [^{125}I]-α-BTX (Perkin-Elmer, Boston, MA) to intact oocytes. Oocytes were incubated in 10 nM [^{125}I]-α-BTX with 5 mg/mL bovine serum albumin in MOR2 buffer (115 mM NaCl, 2.5 mM KCl, 5 mM MgCl$_2$, 1 mM Na$_2$-HPO4, 5 mM HEPES, 0.2 mM CaCl$_2$, pH = 7.4) in a volume of 50 μL for 1.5 h at room temperature. Oocytes were then washed with 20 mL of MOR2 buffer to remove excess toxin. Noninjected oocytes served as background for nonspecific binding. [^{125}I]-α-BTX binding (cpm) of oocytes and the standard curve solutions (0−10 fmol of [^{125}I]-α-BTX) were measured in a gamma counter (Gamma 5500, Beckman). The Student's *t*-test in GraphPad Prism 3.0 was used to determine statistical significance.

Normalized Macroscopic AChR Response. To determine the normalized functional response to ACh, the [^{125}I]-α-bungarotoxin binding assay was performed immediately following voltage clamping. The protocol to normalize the ACh-induced response is to apply a single ACh concentration of 300 μM per oocyte and then normalize the amount of current measured to the toxin binding sites in the oocyte surface (nA/fmol). This ACh concentration was selected on the basis of the dose−response curve of the wild-type *Torpedo* AChR (*11*). This is defined as the peak of the ACh-induced current (nA) per femtomole of surface α-bungaro-toxin binding sites. Using this approach, we can determine the normalized channel response to ACh.
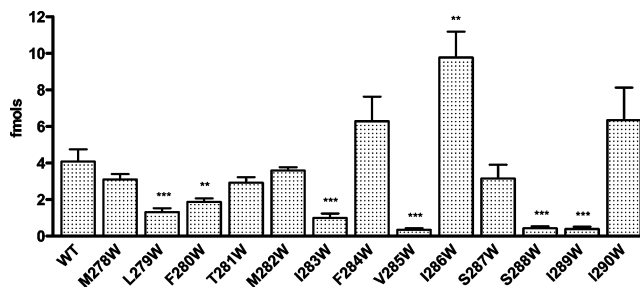

FIGURE 2: Expression of AChR mutants. [^{125}I]-α-BTX binding was used to determine the expression levels of each mutant in *Xenopus* oocytes. Each bar represents the average level of [^{125}I]-α-BTX (fmol) bound to 8−15 oocytes. Higher numbers of oocytes were used to measure BTX binding in the V285W ($n = 30$) and the I289W ($n = 51$) mutants. The L279W, I283W, V285W, S288W, and I289W mutants displayed expression levels that were markedly significantly different (marked ***, meaning $p < 0.001$) than that of wild type. The mutants F280W and I286W displayed expression levels with a more modest significant difference (marked **, meaning $p = 0.001−0.01$) than that of wild type.

RESULTS

Expression of AChR Mutants. Tryptophan-scanning mu-tagenesis was performed on the αM3 of *Torpedo* AChR beginning at residue M278 and extending to I290, as illustrated in Figure 1. *Xenopus* oocytes were injected with mRNA encoding the mutated α subunit and wild-type β, γ, and δ subunits. The expression levels of each mutant were measured by [^{125}I]α-BTX binding, as summarized in Figure 2. Seven mutants (L279W, F280W, I283W, V285W, I286W, S288W, and I289W) exhibited expression levels significantly different than that of wild-type αM3. Of these, V285W, S288W, and I289W were expressed at levels less than 15% of that of wild type. The mutants L279W, F280W, and I283W were expressed at levels between 25 and 50% of that of wild type. Surprisingly, the I286W mutant was expressed at 2.4-fold higher levels than that of wild type, and the F284W and S287W exhibited expression levels similar to that of wild type.

Effects of the αM3 Mutants on the ACh-Induced Currents. The ion channel properties of AChR mutants were tested using a two-electrode voltage clamp following application of six concentrations of ACh (1, 3, 10, 30, 100, and 300 μM), as shown in Figure 3. The purpose of these experiments was to determine whether the various mutants could assemble into functional channels. The ionic current values of the 13 mutants were normalized to their corresponding expression levels (femtomoles), as shown in Table 1. Although all 13 mutants displayed toxin binding, they did not all assemble into functional channels. Three mutations resulted in a loss of receptor function, including M282W, V285W, and I289W. This suggests that the tryptophan side chain alters the conformational changes required for channel assembly or ion channel function. The loss of function implies that these positions may be involved in helix−helix contacts that are required for channel gating.

The ACh-induced responses exhibited by the F280W, I283W, and S288W mutants appeared to have reduced AChR macroscopic currents. However, these mutants were ex-pressed at significantly lower levels than wild type (Figure 2), and thus the normalized response was actually increased. This result is in close agreement with our previous findings in αM4, in which the majority of the mutations that decreased

Table 1: Functional Consequences of αM3 Mutants

nAChR type	EC_{50}	Hill coefficient	normalized response (−nA/fmol)	I_{max} (−nA)	n
WT	21 ± 2	1.33 ± 0.03	622 ± 56	2456 ± 339	12
M278W	74 ± 19***	1.08 ± 0.16	232 ± 25***	870 ± 111***	14
L279W	3.3 ± 0.2***	1.27 ± 0.11	440 ± 57	738 ± 125***	14
F280W	30 ± 4***	1.17 ± 0.05	818 ± 59*	1602 ± 197*	15
T281W	2.9 ± 0.5***	1.11 ± 0.27	80 ± 11***	230 ± 19***	8
M282W	nd	nd	nd	nd	12
I283W	20 ± 3	1.20 ± 0.06	1230 ± 133***	1000 ± 109***	14
F284W	7.2 ± 0.9***	1.63 ± 0.19	484 ± 57	3218 ± 630	13
V285W	nd	nd	nd	nd	30
I286W	21 ± 4	1.16 ± 0.08	481 ± 87	3781 ± 20*	15
S287W	26 ± 2	1.34 ± 0.05	591 ± 95	1651 ± 254	14
S288W	32 ± 4**	1.21 ± 0.06	1789 ± 387***	595 ± 118***	10
I289W	nd	nd	nd	nd	51
I290W	23 ± 3	1.17 ± 0.06	501 ± 77	2536 ± 434	10

[a] Values are given as the mean ± SE. [b] Normalized response for each oocyte was obtained from ACh-induced current at 300 μM divided by femtomoles of the same oocyte. [c] *** means $p < 0.001$, ** means $p = 0.001−0.01$ and * means $P < 0.01−0.05$. [d] nd, no detectable current.
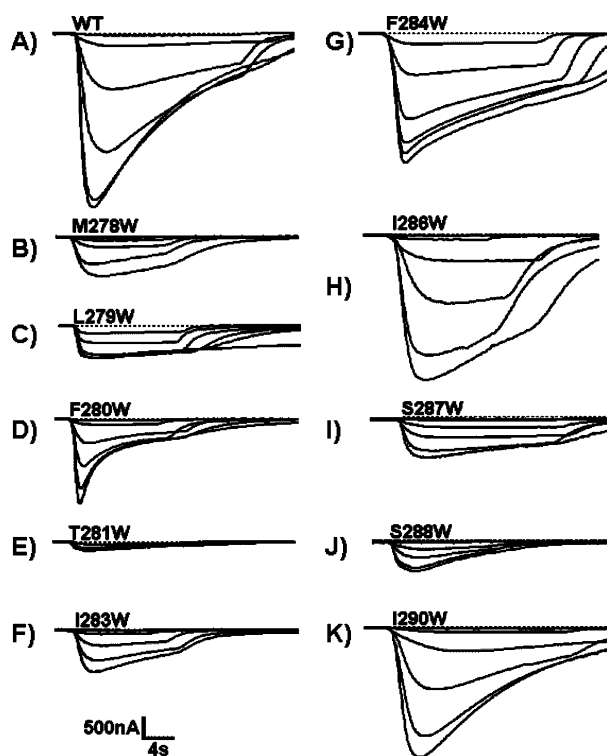

FIGURE 3: Macroscopic current traces of wild-type and αM3 mutants. Macroscopic currents derived from individual oocytes expressing either wild-type or the various αM3 mutant AChRs were recorded using a two-electrode voltage clamp. ACh-induced currents were detected at a membrane potential of −70 mV and filtered at 2 kHz. The ACh concentrations used to generate the family of currents were 1, 3, 10, 30, 100, and 300 μM. After current measurements, [^{125}I]-α-BTX binding was used to measure the expression levels of the various AChRs (in femtomoles). Representative current traces are shown from (A) WT (5.3); (B) M278W (4.4); (C) L279W (1.8); (D) F280W (2.6); (E) T281W (2.3); (F) I283W (0.65); (G) F284W (7.0); (H) I286W (7.5); (I) S287W (2.1); (J) S288W (0.41); and (K) I290W (5.8).

FIGURE 4: Effects of various αM3 mutations on AChR function. Dose−response curves for oocytes expressing either wild-type and or mutant AChRs, including M278W, L279W, F280W, T281W, I283W, F284W, I286W, S287W, S288W, and I290W. Each curve was constructed using ACh-induced currents (nanoamperes) per femtomole of surface α-BTX binding sites. The current values used were collected from peak currents at six concentrations of ACh (1−300 μM). For each ACh concentration, the average ± SEM was estimated from a total of 8−15 oocytes in each group.

the AChR macroscopic currents were associated with low expression levels and higher normalized responses (*13*).

Functional Consequences of AChR Mutants: Effects on the EC_{50}. Dose−response curves for the 10 mutants were performed using a two-electrode voltage clamp (Figure 4), following ACh application. As shown in Figure 3, ion channel currents were recorded using six concentrations of
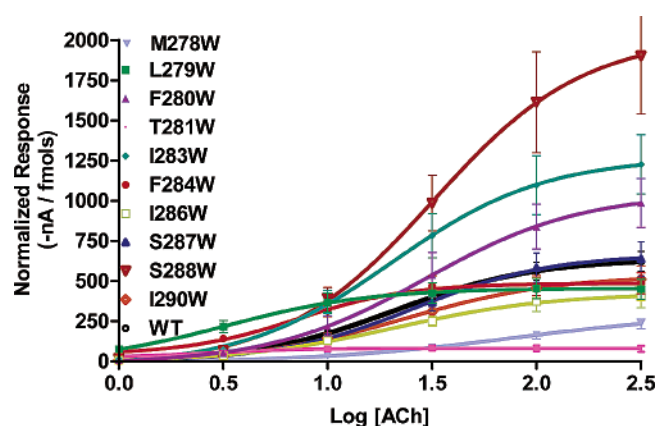
ACh, ranging from 1 to 300 μM. The lipid-exposed mutation F284W decreased the EC_{50} for ACh to 7.2 ± 0.9 μM ($n =$ 13). The mutant M278W reduced the AChR macroscopic currents and increased the EC_{50} value from 21 ± 2 (WT, $n = 12$) to 74 ± 20 μM ($n = 14$). In contrast, the T281W mutant decreased both the EC_{50} to 2.9 ± 0.5 μM ($n = 8$) and the macroscopic currents. The I283W, I286W, S287W, and I290W mutants did not have any significant effect on the EC_{50} values, suggesting that these residues do not alter the gating mechanism of the AChR. Overall, these results suggest that the αM3 is involved in conformational changes of the AChR evoked by ACh binding. The small current size, measured in those mutants with the lowest ACh-induced currents (i.e., M278W, L279W, T281W, I283W, S287W, and S288W), makes it very difficult to evaluate the effect of each mutation on the rapid desensitization using a whole-cell voltage clamp. In general, for those mutants displaying ACh-induced currents similar to or larger than wild-type, desensitization was somewhat slower when compared to wild type.

DISCUSSION

The *Torpedo* M3 transmembrane domain has several residues in contact with the lipid interface (*8*). In the present study, we used tryptophan-scanning mutagenesis to examine the role of 13 residues (from M278 to I290) of the αM3 in AChR channel function. Two lipid-exposed residues (F284 and S287) (*8*) were included in this analysis. We expressed the AChR in *Xenopus laevis* oocytes; the expression levels of the mutants were estimated by [^{125}I]-α-BTX binding assays, and the macroscopic currents were assessed using a two-electrode voltage clamp.

The V285W, S288W, and I289W mutants exhibited the most dramatic reduction in AChR expression, with expression levels less than 15% of that of wild type. We hypothesized that tryptophan substitution at these positions disrupts AChR trafficking, assembly, and/or oligomerization. To test the hypothesis that the receptor may be retained at the interior of the membrane, we homogenized the oocytes expressing these mutations prior to [^{125}I]-α-BTX binding. There was no difference in AChR expression levels between the homogenized versus intact oocytes. These results demonstrated that these mutants do not affect AChR trafficking, suggesting that the efficiency of assembly could cause the reduced expression.

It is of interest to note that the M282W, V285W, and I289W mutants, which exhibited [^{125}I]-α-BTX binding (3.6, 0.34, and 0.27 fmol, respectively), did not show detectable ionic currents. Previous photoaffinity labeling studies have suggested that these residues are located at the interior of the protein (*8*). The M282W mutant exhibited no current in response to 300 μM ACh, but did show significant [^{125}I]-α-BTX binding with similar expression levels as the wild type. These results suggest that the M282 position might face the interior of the protein and may be involved in a critical helix−helix contact that stabilizes the closed state of the AChR channel. It is possible that a tryptophan replacement at the M282 position caused sufficient steric hindrance to restrain the conformational change required for channel gating. We did not detect ACh-induced currents for the V285W and I289W mutants. However, in contrast to M282W, the V285W and I289W mutants were expressed at significantly lower levels as compared to wild type. The aforementioned results suggest that tryptophan substitution at these positions inhibits the efficiency of channel assembly, which could lead to the loss of ion channel function. The V285 site is the critical site not only in the αM3, but also in its analogous position in the β subunit, V291, which exhibited a similar pattern of inhibition (manuscript in preparation). This position was previously characterized in the muscle-type AChR, where a αV285I mutation was shown to mediate congenital myasthenic syndrome. In this elegant study, the authors found that the αV285I mutation causes slow opening and rapid closing rates of the AChR channel (*20*). Taken together, these results suggest that the M282, V285, and I289 positions in αM3 are highly sensitive to increased side-chain volume and that this inhibits channel function. The lack of ionic currents exhibited by these three inhibitory mutations suggests that the αM3 is more tightly packed toward the interior of the protein, as compared to the previously characterized αM4 (*13*). In addition to side-chain volume, it is possible that some mutations, such as T281W, S287W,

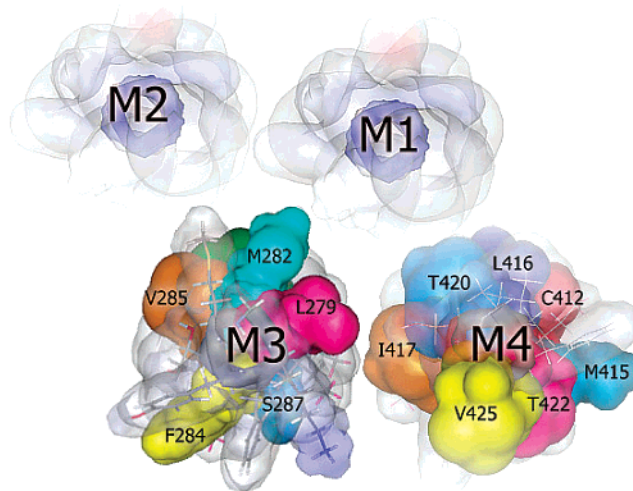FIGURE 5: Hypothetical topological model of the four transmembrane segments for the *Torpedo californica* AChR α-subunit. The structural models for the αM3 and αM4 domains were examined using Biomer V1.0 alpha (see http://www.scripps.edu/n~nwhite/B). The structures were minimized using the Fletcher−Reeves conjugated gradient algorithm (<1000 iterations). Inhibitory positions in the αM3 (M282, V285, and I289) are facing the same side of the helix, oriented toward the M2 domain, while lipid-exposed residues face the opposite side of the helix.

and S288W, may affect hydrogen bond formation. For example, tryptophan replacement at position T281 represents the slightest increase in volume among these mutations yet the largest loss in ion channel function (see Figure 3). This observation suggests that hydrogen bonding of the hydroxyl group at position T281 could be critical for AChR function and/or assembly. A similar pattern was observed for the S287W and S288W mutations. In the αM4 domain, tryptophan replacements at positions L416, I419, and I420 produced the largest reduction in expression levels (0.36, 0.62, and 0.66 fmol, respectively); however, these three mutations all produced a functional AChR (*13*). One possible explanation for these differences is that, within the α subunit, the M3 domains are in more direct contact with the M2 domains, which form the ion channel; perhaps M4 may be more closely in contact with the M1 domain (Figure 5).

The S287W and S288W mutations have the same substitution, yet their effects are significantly different. The S287W mutant showed the same response to ACh, as did the wild type, whereas S288W exhibited a reduction in AChR macroscopic currents. A possible explanation for these results is that S287 is a lipid-exposed residue labeled by [^{125}I]-TID (*8*) and may thereby more easily accommodate the tryptophan, whereas the S288W mutant might be facing toward the interior of the protein. Using ^{1}H NMR spectroscopy to study a synthetic peptide corresponding to αM3 from *Torpedo californica,* Lugovskoy and colleagues proposed that the CO group of the S288 residue forms a stable hydrogen bond with the HO proton of the T292 (*19*). According to this study, the aforementioned hydrogen bond pulls S288, causing its amide proton to form a hydrogen bond with the carboxyl group of V285. It is possible that a tryptophan substitution at S288 leads to a localized distortion of the helix that could affect the orientation of these hydrogen bonds. The disruption of this array of hydrogen bonds could provide

a plausible explanation for the inhibitory behavior exhibited by the S288W mutation.

The lipid-exposed mutation F284W exhibited a decreased EC_{50} for ACh. This mutation showed increased receptor macroscopic currents at low ACh concentrations ($1-30 \mu M$), whereas decreased macroscopic currents were observed at high ACh concentrations ($100-300 \mu M$). The decrease in EC_{50} and the increased macroscopic responses at low ACh concentrations suggest that the F284 modulates AChR channel gating. A possible explanation for the decrease in macroscopic responses at high agonist concentrations exhibited by this mutant could be explained by channel block and/or desensitization. This type of profile was observed in the lipid-exposed V425W mutant in a previous characterization of $\alpha M4$, where channel block decreased the macroscopic response of the V425W mutant (*13*). An analogous tryptophan replacement of this mutation in the *Torpedo* β subunit (F290W) also caused a reduction in the AChR macroscopic currents (manuscript in preparation). In the β subunit, this residue is not lipid-exposed, as it was not labeled by [^{125}I]-TID (*8*). Recently, Bouzat and colleagues examined the analogous position F284W in the mouse AChR and found that in all subunits, this position contributes to channel gating (*22*). The response of the αF284 from *Torpedo* is consistent with the response of its analogous residue in the muscle-type AChR (*22*). This residue can be added to an exclusive group of lipid-exposed positions sensitive to hydrophobic substitutions, including αC418 (*9*), βC447 (*10*), αV425 (*13*), γF292 and γL296 (*21*), and αT422 (*14, 15*).

The normalized macroscopic response for the $\alpha M3$ mutants is shown in Table 1. The three mutants that showed the highest normalized responses, F280W, I283W, and S288W, all had low AChR expression levels. Of these mutations, F280W and S288W exhibited the largest EC_{50} values as compared to wild type, and I283W displayed an EC_{50} value similar to that of wild type. As shown in Figure 2, the I283W and S288W mutations, which were expressed at significantly lower levels than the wild-type AChR (1.0 and 0.4 fmol, respectively), appear to have the highest normalized response of all the mutations examined. This is not simply due to the low number of BTX binding sites, because some of our previous mutations with low expression levels did not exhibit normalized responses higher than wild type; for example, V423W in the $\alpha M4$ displayed a normalized response of 809 nA/fmol (*13*). Furthermore, mutations that were expressed at the same level as wild type showed responses lower than wild type (i.e., M278W and T281W) and responses similar to wild type (i.e., S287W and I290W). In summary, the pattern of normalized responses in $\alpha M3$ is similar to those found in our previous studies of the $\alpha M4$ (*13*), $\gamma M3$ (*21*), and ongoing studies in the $\beta M3$ domains, where receptor function seems to be dependent on the mutant itself rather than due to variation in expression levels.

STRUCTURAL INTERPRETATION

Although the overall spatial organization of the *Torpedo* electric organ AChR was deduced a decade ago (*24*), the secondary structure of the transmembrane domains remains to be established. Hydrophobicity plots suggested an α-helical structure for the four transmembrane domains (*4, 25*). The overall three-dimensional structure of *Torpedo* AChR

at 9-Å resolution, deduced from cryomicroscopy, suggests that a single α helix in each of the subunits forms the M2 domain that lines the channel pore. The lack of similar density of the lipid-facing portion of the AChR was interpreted as a possible β structure for the M1, M3, and M4 domains (*24*). Various studies using Fourier transformed infrared spectroscopy (FTIR) suggested that all transmembrane segments of the *Torpedo* AChR are largely α-helical (*26-28*). Photoaffinity labeling studies of the M3 and M4 domains suggested an α-helical structure (*7, 8*). Three-dimensional ^{1}H NMR studies of a synthetic peptide corresponding to the $\alpha M3$ transmembrane domain of *Torpedo* suggested that the region from residues L279 to N297 forms a right-handed helix (*19*). While these studies provided important structural information, they have not delineated the secondary structures of the transmembrane domains.

Tryptophan-scanning mutagenesis is a useful method for predicting structural patterns and functional features, and this approach has been used to characterize transmembrane proteins such as the Na$^+$$-K^+$ ATPase (*29*), the MotA proton channel (*30, 31*), the GABA$_A$ receptor α_2M2 transmembrane domain (*32*), and recently the α_1M4 (*33*). Because the three-dimensional structure of the AChR is unknown, our laboratory has previously used tryptophan-scanning analysis to predict structural patterns of the $\alpha M4$ (*13*) and $\beta M3$ (manuscript in preparation) domains, and we have now used this approach to characterize the $\alpha M3$ domain.

The periodicity of changes in the expression levels of AChR could be associated with either the resting or closed conformation of the AChR, given that activation of the ion channel is not required for determining the number of surface receptors. On the other hand, the periodicity of the functional response of the AChR could be associated with the activated state of the channel, given that EC_{50} values are estimated from macroscopic current analysis. It has been well established that the AChR undergoes a substantial conformational change during the transition from the closed to the open state and that this conformational change propagates through the α subunits (*34, 35*). However, it is not known how this conformational change propagates to other structural domains of the AChR.

The periodicity of changes in the functional response and the normalized expression levels of the $\alpha M3$ are shown in Figure 6. To get a clearer picture of the steric disruption caused by the tryptophan substitutions, we normalized the AChR expression levels to the net change in volume per position (see Figure 6A). We found that the normalized analysis (femtomoles per volume change) provides a sharper oscillatory pattern when compared to the non-normalized expression plot. A plausible explanation for this observation is that the transmembrane segments of the AChR are tightly packed and side-chain volume is critical for the heteropentamer assembly and ion channel function. This type of analysis thus provides a better approximation of how the net volume changes, caused by tryptophan replacement, affect the expression of AChRs. We estimated a ratio of the femtomoles of AChR expressed by each mutant with respect to the changes in volume caused by the tryptophan substitution on each residue. The values used for the volume of amino acid residues were those reported by Chothia in 1975 (*36*). The oscillation of the functional consequences and the
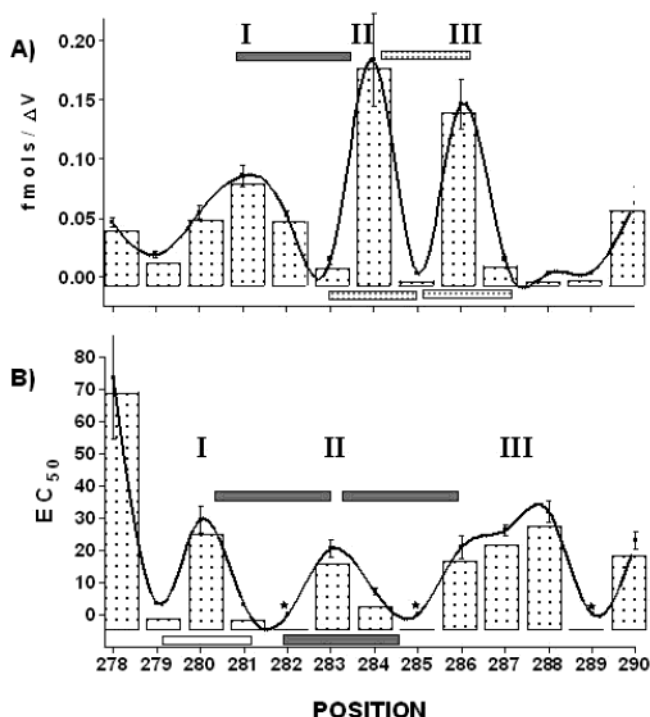
FIGURE 6: Periodicity of changes in AChR-normalized expression levels and function plotted as a function of tryptophan substitutions in the αM3. (A) The plot for the normalized expression levels (the femtomoles of AChR expressed by each mutant as a ratio of the changes in volume caused by the tryptophan substitution). (B) EC_{50} values are shown for each position, to illustrate the functional effects of each mutation. Both plots were constructed using a cubic spline curve regression function (GraphPad software). Individual sets of data for the normalized expression and the EC_{50} for each αM3 AChR mutant are shown in bars with dots. The asterisks indicate the M282W, V285W, and I289W mutants which did not form a functional AChR. The oscillations of the curves suggest an average periodicity close to 3.6 (gray bars) amino acids. Although the average periodicity was 3.6, in the close or resting conformation the periodicity appears to be 3.0 in phases II and III (dotted bars). This value was estimated by performing the first derivative for each amino acid position and estimating the distance between the zeros for all positions using GraphPad software. Each point on the *Y*-axis represents an average of a number of measurements.

expression levels as a function of the αM3 residues 278−290 indicates an α-helical structure.

Three distinct phases are evident in both oscillatory analyses and channel conformations for 11 positions between L279 and I290 (Figure 6A, B). The periodicity value was estimated by performing the first derivative for each amino acid position and estimating the distance between the zeros for all positions using GraphPad software. The oscillatory pattern for both conformations shows an average periodicity of 3.6 amino acids per oscillation. In the closed or resting conformation, phase I, which includes residues 279−282, seems to be compatible with an α-helical structure, whereas phases II and III residues (283−287) display a periodicity of about 3.0, which could be consistent with a 3_{10}-helical structure. The oscillatory pattern for the channel-activated state of the AChR shown in Figure 6B shows a pattern more consistent with an α-helical structure; however, in phase III at positions S287 and S288, the periodicity is less well-defined. This disruption of the periodicity could be due to the dramatic change in volume caused by the tryptophan itself, and this could lead to alterations in hydrogen bonding

between the amino acid side chains, leading to a distortion of the proposed α-helix.

Interestingly, the ^1H NMR spectroscopy study of a synthetic peptide corresponding to the αM3 from *Torpedo californica* by Lugovskoy and colleagues further confirms that this region contains a mixture of different helical conformations (*19*). Specifically, the first turn (residues L279−M282) was proposed to be a 3_{10}-helix, followed by an intermediate conformation of α and 3_{10}-helices that extends to I289. It is possible that the structural information obtained from a two-dimensional ^1H NMR data of a single αM3 peptide may represent an average of the structure of this AChR transmembrane domain in both the open and closed conformations.

In conclusion, our electrophysiological analysis of the αM3 mutants defined key positions critical to the AChR assembly and function. The present study further confirms that the αM3 domain is involved in the overall AChR conformational change evoked by ACh binding. Taken together, these findings provide additional evidence supporting the hypothesis that αM3 is an α-helical structure.

REFERENCES

1. Corringer, P. J., Le Novere, N., and Changeux, J. P. (2000) *Annu. Rev. Pharmacol. Toxicol. 40*, 431−458.
2. Karlin, A., and Akabas, M. H. (1995) *Neuron 15*, 1231−1244.
3. Unwin, N. (1998) *J. Struct. Biol. 121*, 181−190.
4. Noda, M., Takahashi, H., Tanabe, T., Toyosato, M., Kikyotani, S., Furutani, Y., Hirose, T., Takashima, H., Inayama, S., Miyata, T., and Numa, S. (1983) *Nature 302*, 528−532.
5. Hucho, F., Tsetlin, V. I., and Machold, J. (1996) *Eur. J. Biochem. 239*, 539−557.
6. Akabas, M. H., and Karlin, A. (1995) *Biochemistry 34*, 12496−12500.
7. Blanton, M. P., and Cohen, J. B. (1992) *Biochemistry 31*, 3738−3750.
8. Blanton, M. P., and Cohen, J. B. (1994) *Biochemistry 33*, 2859−2872.
9. Lee, Y. H., Li, L., Lasalde, J., Rojas, L., McNamee, M., Ortiz-Miranda, S. I., and Pappone, P. (1994) *Biophys. J 66*, 646−653.
10. Lasalde, J. A., Tamamizu, S., Butler, D. H., Vibat, C. R., Hung, B., and McNamee, M. G. (1996) *Biochemistry 35*, 14139−14148.
11. Ortiz-Miranda, S. I., Lasalde, J. A., Pappone, P. A., and McNamee, M. G. (1997) *J. Membr. Biol. 158*, 17−30.
12. Tamamizu, S., Lee, Y., Hung, B., McNamee, M. G., and Lasalde-Dominicci, J. A. (1999) *J. Membr. Biol. 170*, 157−164.
13. Tamamizu, S., Guzman, G. R., Santiago, J., Rojas, L. V., McNamee, M. G., and Lasalde-Dominicci, J. A. (2000) *Biochemistry 39*, 4666−4673.
14. Bouzat, C., Roccamo, A. M., Garbus, I., and Barrantes, F. J. (1998) *Mol. Pharmacol. 54*, 146−153.
15. Bouzat, C., Barrantes, F., and Sine, S. (2000) *J. Gen. Physiol. 115*, 663−672.
16. Bouzat, C., Gumilar, F., del Carmen Esandi, M., and Sine, S. M. (2002) *Biophys. J. 82*, 1920−1929.
17. Giraudat, J., Montecucco, C., Bisson, R., and Changeux, J. P. (1985) *Biochemistry 24*, 3121−3127.
18. Campos-Caro, A., Rovira, J. C., Vicente-Agullo, F., Ballesta, J. J., Sala, S., Criado, M., and Sala, F. (1997) *Biochemistry 36*, 2709−2715.
19. Lugovskoy, A. A., Maslennikov, I. V., Utkin, Y. N., Tsetlin, V. I., Cohen, J. B., and Arseniev, A. S. (1998) *Eur. J. Biochem. 255*, 455−461.
20. Wang, H. L., Milone, M., Ohno, K., Shen, X. M., Tsujino, A., Batocchi, A. P., Tonali, P., Brengman, J., Engel, A. G., and Sine, S. M. (1999) *Nat. Neurosci. 2*, 226−233.
21. Cruz-Martin, A., Mercado, J. L., Rojas, L. V., McNamee, M. G., and Lasalde-Dominicci, J. A. (2001) *J. Membr. Biol. 183*, 61−70.

22. De Rosa, M. J., Rayes, D., Spitzmaul, G., and Bouzat, C. (2002) *Mol. Pharmacol. 62*, 406−414.

23. Ho, S. N., Hunt, H. D., Horton, R. M., Pullen, J. K., and Pease, L. R. (1989) *Gene 77*, 51−59.

24. Unwin, N. (1993) *Cell 72 Suppl*, 31−41.

25. Claudio, T., Ballivet, M., Patrick, J., and Heinemann, S. (1983) *Proc. Natl. Acad. Sci. U.S.A. 80*, 1111−1115.

26. Baenziger, J. E., and Methot, N. (1995) *J Biol Chem 270*, 29129−29137.

27. Methot, N., and Baenziger, J. E. (1998) *Biochemistry 37*, 14815−14822.

28. Baenziger, J. E., Morris, M. L., Darsaut, T. E., and Ryan, S. E. (2000) *J. Biol. Chem. 275*, 777−784.

29. Hasler, U., Crambert, G., Horisberger, J. D., and Geering, K. (2001) *J. Biol. Chem. 276*, 16356−16364.

30. Sharp, L. L., Zhou, J., and Blair, D. F. (1995) *Biochemistry 34*, 9166−9171.

31. Sharp, L. L., Zhou, J., and Blair, D. F. (1995) *Proc. Natl. Acad. Sci. U.S.A. 92*, 7946−7950.

32. Ueno, S., Lin, A., Nikolaeva, N., Trudell, J. R., Mihic, S. J., Harris, R. A., and Harrison, N. L. (2000) *Br. J. Pharmacol. 131*, 296−302.

33. Jenkins, A., Andreasen, A., Trudell, J. R., and Harrison, N. L. (2002) *Neuropharmacology 43*, 669−678.

34. Grosman, C., Zhou, M., and Auerbach, A. (2000) *Nature 403*, 773−776.

35. Williams, D. B., and Akabas, M. H. (1999) *Biophys. J. 77* (5) 2563−2574.

36. Chothia, C. (1975) *Nature 254*, 304−308.